nature communications

Article

https://doi.org/10.1038/s41467-025-57383-8

Liver fibrosis negatively impacts in vivo gene transfer to murine hepatocytes

Received: 4 March 2024

Accepted: 20 February 2025

Published online: 10 March 2025

Check for updates

Chiara Simoni[1,2], Justine Nozi[3,4], Francesco Starinieri[1], Tiziana La Bella[3,4], Elisabetta Manta[1], Camilla Negri[1], Mauro Biffi[1], Rossana Norata[1], Martina Rocchi[5], Francesca Sanvito[1,5], Giuseppe Ronzitti[3,4], Elena Barbon[1] ✉ & Alessio Cantore[1,2] ✉

Liver fibrosis occurs in several genetic and acquired disease conditions, leading to alterations of the tissue and metabolism, which may adversely affect viral vector-mediated gene therapy. Here, we assessed the impact of liver fibrosis on in vivo gene transfer to hepatocytes mediated by lentiviral vectors or adeno-associated viral vectors. We exploited two chemically induced fibrosis mouse models characterized by tissue damage in different areas of the liver lobule. Moreover, we used *Abcb11*$^{-/-}$ and *Agl*$^{-/-}$ mice, recapitulating features of inherited cholestasis and glycogen storage disease, as representative models of genetic disorders characterized by liver fibrosis. We report a general negative influence of liver fibrosis on hepatocyte transduction and alteration of the vector distribution within the liver lobule, with different outcomes according to the viral vector used and the state of the liver at the time of vector administration. This study bears implications for future developments and applications of in vivo liver-directed gene therapy.

Liver fibrosis is a pathological wound healing resulting in a progressive substitution of the damaged parenchyma with scar tissue composed of extracellular matrix elements such as collagen[1]. This pathological mechanism can develop in several inherited metabolic diseases in which the underlying enzymatic defect leads to hepatocyte damage[2]. Early onset of fibrosis is typical in disorders of bile acid metabolism, such as progressive familial intrahepatic cholestasis types 2 and 3 (PFIC-2 and PFIC-3)[3]. Liver fibrosis can also develop in other genetic conditions, such as disorders of carbohydrate, lipid, and amino acid metabolism[2]. Besides monogenic diseases, hepatic fibrosis often occurs in several acquired conditions, such as viral hepatitis, alcoholic and metabolic-associated steatohepatitis, or cholestatic injuries[4]. The extracellular matrix deposition and the chronic inflammatory state characterizing the fibrotic status can alter tissue architecture, blood supply, and cellular metabolism, with a potential negative impact on therapeutic approaches targeting the liver.

Liver-directed gene therapy by viral vectors is promising to treat inherited liver diseases since it may allow for restoration of hepatic function by delivering a therapeutic transgene through a single intravenous (i.v.) administration[5]. In recent years, some liver-directed gene therapies have demonstrated clinical efficacy and safety in adult individuals affected by hemophilia. These approaches rely on gene replacement by adeno-associated viral (AAV) vectors delivering a functional copy of the therapeutic transgene[6,7]. Additional AAV vector-based gene therapy strategies are under pre-clinical or clinical evaluation for other monogenic disorders such as Crigler-Najar, Glycogen storage diseases, and Wilson disease, among others[8]. While AAV vectors have shown long-lasting transgene expression in adult individuals, HIV-derived lentiviral vectors (LV) may be better suited for treating young patients in which the liver is actively growing. Indeed, LV stably integrates its cargo into the host genome and is maintained upon cell proliferation, thus potentially allowing long-term transgene expression by a single administration, even to pediatric patients[9–12].

[1]San Raffaele Telethon Institute for Gene Therapy, IRCCS San Raffaele Scientific Institute, Milan, Italy. [2]Vita Salute San Raffaele University, Milan, Italy. [3]Généthon, Évry, France. [4]Université Paris-Saclay, Univ Évry, Inserm, Généthon, Integrare Research Unit UMR_S951, Évry, France. [5]Pathology Unit, IRCCS San Raffaele Scientific Institute, Milan, Italy. ✉e-mail: barbon.elena@hsr.it; cantore.alessio@hsr.it

Determining whether viral-vector mediated gene transfer is affected by liver fibrosis is relevant for liver-directed gene therapy applications, not only for the treatment of diseases characterized by liver fibrosis per se but also when liver fibrosis is a co-morbidity in other diseases such as hemophilia[13]. Moreover, this assessment would also be relevant in the context of liver gene therapy approaches meant to counteract or even revert acquired hepatic fibrosis[14–16].

There are available mouse models of liver fibrosis, both chemically induced and genetic. We exploited carbon tetrachloride (CCl_4) and the 3,5-diethoxycarbonyl-1,4-dihydrocollidine (DDC) to induce liver fibrosis in wild-type (WT) mice. The first is a well-established model of toxic pericentral fibrosis due to the formation of reactive oxygen species upon catabolism of CCl_4 by the cytochrome P450[17]. The latter is a model of cholestatic damage due to obstruction of bile ducts, leading to cholangiocyte activation and ductular proliferation around the portal area[18]. As representative genetic mouse models of fibrosis, we exploited *Abcb11*$^{-/-}$ and *Agl*$^{-/-}$ mice. *Abcb11*$^{-/-}$ mice are a model of PFIC-2, an inborn error of metabolism caused by a lack of bile salt export pump activity. *Abcb11*$^{-/-}$ mice show progressive liver damage due to intrahepatic cholestasis, resulting in periportal fibrosis in adulthood[19]. Notably, fibrosis is worse in PFIC-2 patients than in *Abcb11*$^{-/-}$ mice, in which compensatory genes contribute to bile secretion[19]. *Agl*$^{-/-}$ mice are a model of glycogen storage disorder type III (GSDIII), a metabolic disorder due to deficiency of the glycogen debranching enzyme and resulting in impaired glycogen degradation[20]. *Agl*$^{-/-}$ mice display whole-body glycogen accumulation, low blood glucose, muscle weakness, and mild liver fibrosis, recapitulating the GSDIII clinical phenotype in humans[20,21].

Here, we systematically assess the efficiency of in vivo gene transfer to hepatocytes by both LV and AAV vectors in the presence of different types and stages of liver fibrosis. We report a general negative impact on liver transduction, with differences between AAV vector and LV platforms depending on the type and extent of the pre-existing fibrosis.

Results

CCl_4-induced liver fibrosis negatively affects LV but not AAV vector transduction

To induce liver fibrosis, we administered WT mice with CCl_4 diluted in corn oil for 6 weeks. During CCl_4 treatment, we measured serum levels of alanine transaminase (ALT) and aspartate transaminase (AST) and observed an increase in both liver enzymes over time (ALT > 3000 U/L; AST > 2000 U/L), thus indicating the occurrence of liver damage (Supplementary Fig. 1a, b). In CCl_4-treated mice, we observed moderate pericentral fibrosis with incomplete and complete fibrous septa, occasionally bridging between central veins, and mild inflammatory cell infiltration in the liver capsule (Fig. 1a and Supplementary Table 1). No major alterations were observed in untreated controls (Supplementary Table 1). One week after the last CCl_4 injection, we administered LV (vesicular stomatitis virus glycoprotein, VSV.G-pseudotyped) or AAV vectors (serotype 8) to both CCl_4-treated and untreated control mice (Fig. 1b). These vectors express either a secreted reporter transgene (human FIX, hFIX) or a fluorescent reporter transgene (mCherry) under the control of previously described hepatocyte-specific expression cassettes and are referred to hereafter as LV.hFIX, LV.mCherry, AAV.hFIX and AAV.mCherry (Supplementary Fig. 1c)[12,22]. We selected LV and AAV vector doses expected to achieve 5–20% of liver transduction based on previous experience[12,23]. We longitudinally monitored hFIX amounts in the plasma of treated mice and collected livers at the end of the experiment to determine mCherry expression and vector copies *per* diploid genome (vector genome copy number, VCN) 4 weeks after vector administration (see Fig. 1b). In LV-treated animals, we observed between 3- and 4-fold lower hFIX output in CCl_4-treated mice compared to controls (Fig. 1c), with a statistically significant difference, paralleled by a reduction of LV VCN in the liver (Supplementary Fig. 1d). We also observed a significantly 2-fold lower mCherry-positive liver area in CCl_4-treated mice compared to controls (Fig. 1d, Supplementary Fig. 1e), without detectable difference in LV VCN in the liver (Supplementary Fig. 1f). Regarding the cohort of animals treated with AAV vectors, we report data for males (M) and females (F) separately since the transduction efficiency is known to be different between the two sexes[24]. In both male and female groups, when comparing mice treated or not with CCl_4, we did not detect differences in circulating hFIX (Fig. 1e), mCherry-positive liver area (Fig. 1f and Supplementary Fig. 1g), or AAV VCN in the liver (Supplementary Fig. 1h, i). We evaluated the potential negative impact of vector transduction per se on liver fibrosis induced by CCl_4 by performing histopathology analysis of the livers of mice after LV or AAV administration (see Fig. 1b). We did not observe any worsening of the liver damage (Supplementary Table 1). To exclude a non-specific effect of corn oil administration on LV and AAV vector liver transduction, we performed an additional experiment, including a control group of WT mice treated with corn oil alone for 6 weeks. As in the previous experiment, we administered LV.mCherry or AAV.mCherry and collected livers 4 weeks after vector administration (Supplementary Fig. 2a). Treatment with corn oil alone did not result in any increase of serum liver enzymes, while liver damage was confirmed in the CCl_4-treated group (Supplementary Fig. 2b, c). Regarding LV-injected mice, we confirmed the reduction in the mCherry-positive liver area and VCN when employing CCl_4, while we did not observe any significant reduction in mice treated with corn oil alone (Supplementary Fig. 2d, e). In the cohort administered with AAV vector, we confirmed no major impact of CCl_4 or corn oil treatment on AAV vector liver transduction, as assessed by measuring mCherry-positive liver area and VCN (Supplementary Fig. 2f, g). These data show that CCl_4-induced pericentral fibrosis caused a reduction in the efficiency of gene transfer into hepatocytes by LV but not AAV vectors.

DDC-induced biliary fibrosis negatively affects both LV and AAV vector transduction

We fed WT mice with a DDC-supplemented diet for 5 weeks to induce biliary liver fibrosis. A control group was fed in parallel with a standard rodent diet without adding the DDC compound. In DDC-fed mice, we observed an elevation of serum ALT and AST (>1000 U/L), indicating liver damage (Supplementary Fig. 3a, b). The damage resulted in cholestasis, marked periportal fibrosis with complete septa bridging between portal areas, and mild to moderate periductular inflammatory cell infiltrate (Fig. 2a and Supplementary Table 2). We did not detect alterations in control mice fed with the standard diet (Supplementary Table 2). One week after the end of this dietary regimen, we administered LV.hFIX, LV.mCherry, AAV.hFIX, or AAV.mCherry to DDC-fed and control mice (Fig. 2b). We longitudinally monitored hFIX amounts in the plasma and collected livers 4 weeks after vector administration to determine mCherry expression and VCN (Fig. 2b). In LV-injected animals when comparing DDC-fed mice and controls, we observed around 10-fold reduction in hFIX output at the last time of analysis and a 4.5-fold reduction in the mCherry-positive liver area (Fig. 2c, d and Supplementary Fig. 3c). This was paralleled by similar or lower LV VCN in the liver (Supplementary Fig. 3d, e). In both male and female AAV vector-injected animals, we observed lower circulating hFIX (Fig. 2e) and mCherry-positive liver area (Fig. 2f and Supplementary Fig. 3f) in DDC-treated mice compared to controls. Note that the control groups shown in Fig. 2f are the same as the ones reported in Fig. 1f. Indeed, to reduce the number of experimental animals, we treated in parallel control mice with those pretreated with either CCl_4 or DDC (see Figs. 1f and 2f). Since male and female mice received the same treatment in parallel and thus belong to the same

https://doi.org/10.1038/s41467-025-57383-8

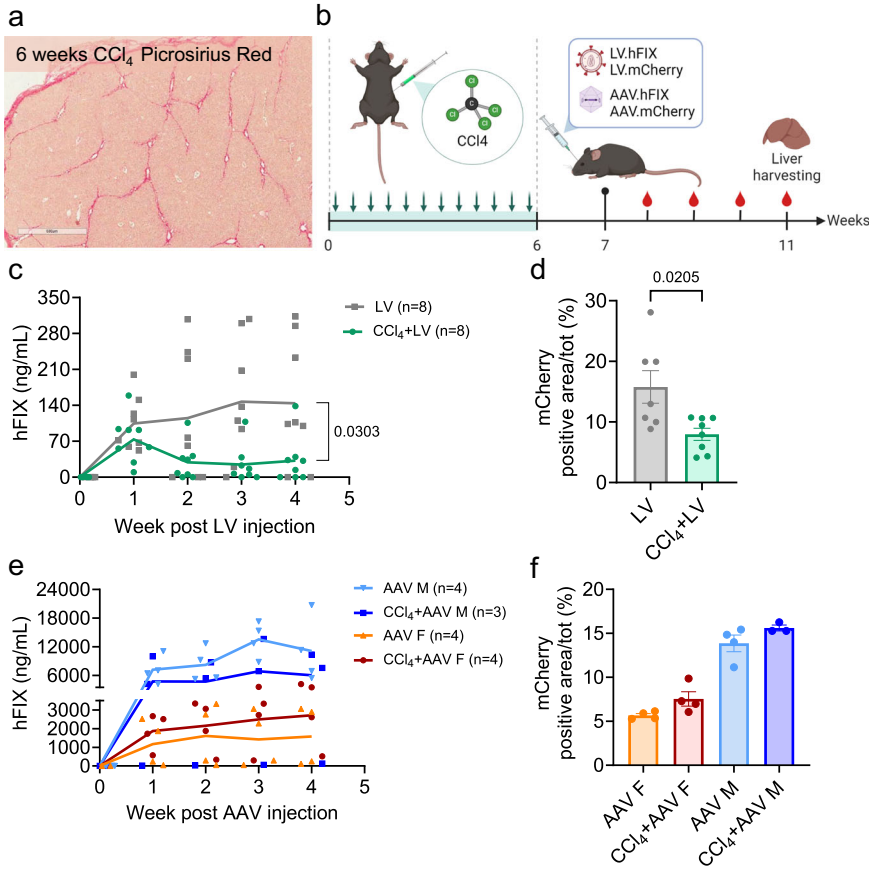

Fig. 1 | CCl_4-induced liver fibrosis negatively affects LV but not AAV vector transduction. a Representative histological image of a liver section from mice ($n = 12$) treated with CCl_4 for 6 weeks (bar = 600 μm). Picrosirius red staining. **b** Schematics of experimental design with timeline (green arrows indicate CCl_4 administrations, red drops indicate blood collections). LV.hFIX and LV.mCherry 3.5×10^{10} transducing units (TU)/kg. AAV.hFIX 5×10^{11} vector genomes (vg)/kg. AAV.mCherry 1×10^{11} vg/kg. Created with BioRender (https://BioRender.com/x47z362). **c** Individual values with mean of hFIX concentration in the plasma of experimental mice at the indicated time after vector administration (Mann–Whitney test at the last time point). Gray symbols indicate mice treated with LV only ($n = 8$), and green symbols indicate mice treated with CCl_4 and LV ($n = 8$). **d** Individual values and mean ± SEM of percentage (%) of mCherry-positive liver area expressed over the total area analyzed (Mann–Whitney test). Gray symbols indicate mice treated with LV only ($n = 7$), and green symbols indicate mice treated with CCl_4 and LV ($n = 8$). **e** Individual values with mean of hFIX concentration in the plasma of experimental mice at the indicated time after vector administration. Light blue symbols indicate male (M) mice treated with AAV only ($n = 4$), blue symbols indicate male mice treated with CCl_4 and LV ($n = 3$), orange symbols indicate female (F) mice treated with AAV only ($n = 4$), red symbols indicate female mice treated with CCl_4 and LV ($n = 4$). **f** Individual values and mean ± SEM of percentage (%) of the mCherry-positive liver area expressed over the total area analyzed. Orange symbols indicate female mice treated with AAV only ($n = 4$), red symbols indicate female mice treated with CCl_4 and LV ($n = 4$), Light blue symbols indicate male mice treated with AAV only ($n = 4$), blue symbols indicate male mice treated with CCl_4 and LV ($n = 3$). Source data are provided as a Source Data file.

experimental cohort, we normalized the values of these two data sets with the mean of their respective controls to perform statistical analysis. We observed a statistically significant reduction in transgene output (Fig. 2g, h) and AAV VCN in the liver of DDC-fed mice (Supplementary Fig. 3g–j). As for the CCl_4 fibrosis model, we did not observe any worsening of the DDC-induced liver damage after LV or AAV administration (Supplementary Table 2). These data indicate that DDC-induced periportal fibrosis considerably reduced the efficiency of hepatocyte gene transfer by both LV and AAV vectors.

Liver fibrosis impacts on LV transduction of hepatocytes without major alteration of LV biodistribution

In the above-described experiments employing LV, VCN analysis is not always concordant with transgene output (for example, see Fig. 1d and Supplementary Fig. 1f). This discrepancy is due to the ability of LV to transduce many different liver cell types[12]. Therefore, VCN results from the contribution of various cells that are transduced. On the other hand, the transgene is expressed only by hepatocytes since we use a hepatocyte-specific expression cassette (see Supplementary Fig. 1c). To address this issue, we performed an in vivo study in the CCl_4 and DDC mouse models, in which we evaluated the LV biodistribution in liver cell subpopulations and major organs. We administered CCl_4 for 6 weeks and the DDC diet for 5 weeks to WT mice. One week after the end of the treatment, we injected LV.hFIX or LV.mCherry, and collected blood 30 min, 60 min, and 24 h post-injection to monitor the clearance of LV in circulation (Fig. 3a). Then, we longitudinally monitored hFIX transgene and 5 weeks after LV injection we harvested major organs and purified hepatocytes, Kupffer cells (KC), liver sinusoidal endothelial cells (LSEC), and hepatic stellate cells (HSC) from the liver by fluorescence-activated cell sorting (FACS) for VCN analysis (Fig. 3a). We confirmed the induction of liver damage by elevation of serum ALT, AST (>1500 U/L for DDC and >3000 U/L for CCl_4; Supplementary Fig. 4a, b), and alkaline phosphatase (ALP), elevated just in the presence of biliary damage (>500 U/L for DDC; Supplementary Fig. 4c). We confirmed the reduction of hFIX output and mCherry-positive hepatocytes in CCl_4 and DDC-treated mice compared to controls (Fig. 3b–d). In the blood, we observed a similar amount of LV Gag p24 capsid protein after LV.hFIX and LV.mCherry injection in all groups, suggesting no major impact of CCl_4 and DDC treatment on the clearance of LV (Supplementary Fig. 4d–f). We then assessed VCN in

https://doi.org/10.1038/s41467-025-57383-8

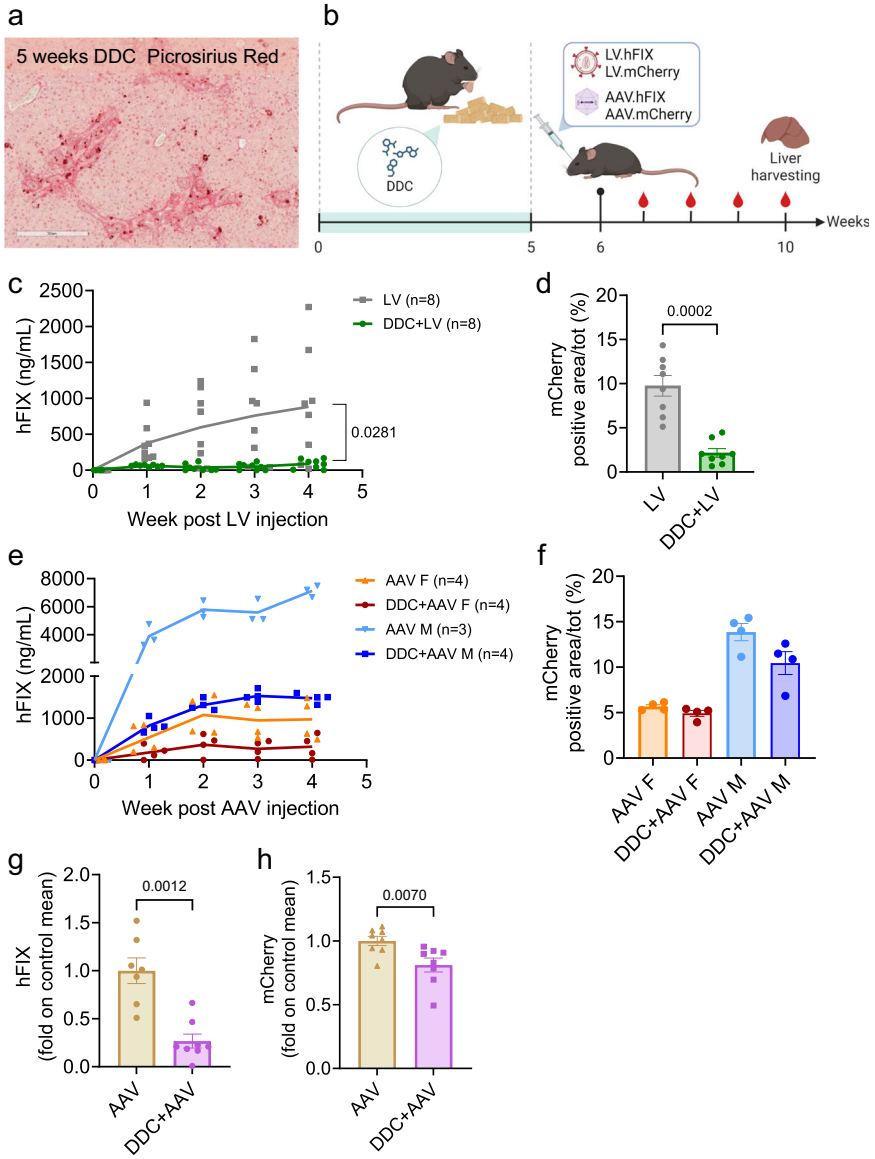

Fig. 2 | DDC-induced biliary fibrosis negatively affects both LV and AAV vector transduction. a Histological image of liver section from mice ($n = 10$) fed with a DDC-supplemented diet for 5 weeks (bar = 300 μm). Picrosirius red staining. **b** Schematics of experimental design (green bar indicates DDC diet) created with BioRender (https://BioRender.com/k46g488). LV.hFIX 5×10^{10} TU/kg. LV.mCherry 3.5×10^{10} TU/kg. AAV.hFIX 2×10^{11} vg/kg. AAV.mCherry 1×10^{11} vg/kg. **c** Individual values with mean of hFIX concentration in the plasma. (Mann–Whitney test at the last time point). Gray and green symbols indicate mice treated with LV only ($n = 8$) or with DDC and LV ($n = 8$), respectively. **d** Individual values and mean ± SEM of percentage (%) of mCherry-positive liver area over the total area analyzed (Mann–Whitney test). Gray and green symbols indicate mice treated with LV only ($n = 8$) or with DDC and LV ($n = 8$), respectively. **e** Individual values with mean of hFIX concentration in the plasma. Orange symbols indicate female mice treated with AAV only ($n = 4$), red symbols indicate female mice treated with DDC and LV ($n = 4$), light blue symbols indicate male mice treated with AAV only ($n = 3$), blue symbols indicate male mice treated with DDC and LV ($n = 4$). **f** Individual values and mean ± SEM of percentage (%) of mCherry-positive liver area over the total area analyzed. AAV F and AAV M are the same data displayed in Fig. 1f, shown here for comparison. Orange symbols indicate female mice treated with AAV only ($n = 4$), red symbols indicate female mice treated with DDC and LV ($n = 4$), light blue symbols indicate male mice treated with AAV only ($n = 4$), blue symbols indicate male mice treated with DDC and LV ($n = 4$). **g**, **h** Individual values with mean ± SEM of hFIX concentration at the last time point analyzed (**g** row data displayed in (**e**)) or % of mCherry-positive liver area (**h** row data displayed in (**f**)) expressed as fold on the mean of each respective control group (Mann–Whitney test). Brown and purple symbols indicate mice treated with AAV only (for hFIX $n = 7$, for mCherry $n = 8$) or with DDC and AAV ($n = 8$), respectively. Source data are provided as a Source Data file.

different organs. We observed a significant reduction of liver LV VCN and a trend of decrease in spleen LV VCN in mice with liver damage (Fig. 3e–g). We found very low to undetectable VCN in kidney, lung, heart, and brain in all mice (Fig. 3e–g). We then FACS-sorted hepatocytes KC, LSEC, and HSC (Supplementary Fig. 4g, h) and confirmed that VCN measured in hepatocytes paralleled the transgene output. Indeed, regarding LV.hFIX, we observed a 1.5-fold reduction in hepatocyte VCN in CCl_4-treated mice and a 9.6-fold reduction in DDC-treated mice (Fig. 3h). Regarding LV.mCherry, we observed a significant 2.3- and a 4.9-fold reduction in hepatocyte VCN in CCl_4– and DDC-treated mice, respectively (Fig. 3i, j). We detected VCN in all the liver cell populations without notable differences between the treatment groups (see Fig. 3h–j). These data confirmed that liver gene transfer is reduced in the presence of CCl_4– and DDC-induced fibrosis and suggest that the spleen's transduction is also impacted. Specifically, we found that the reduced transgene output was due to a reduction in the transduction of hepatocytes, regardless of the transgene used, without major changes in the transduction of other liver cell types.

https://doi.org/10.1038/s41467-025-57383-8

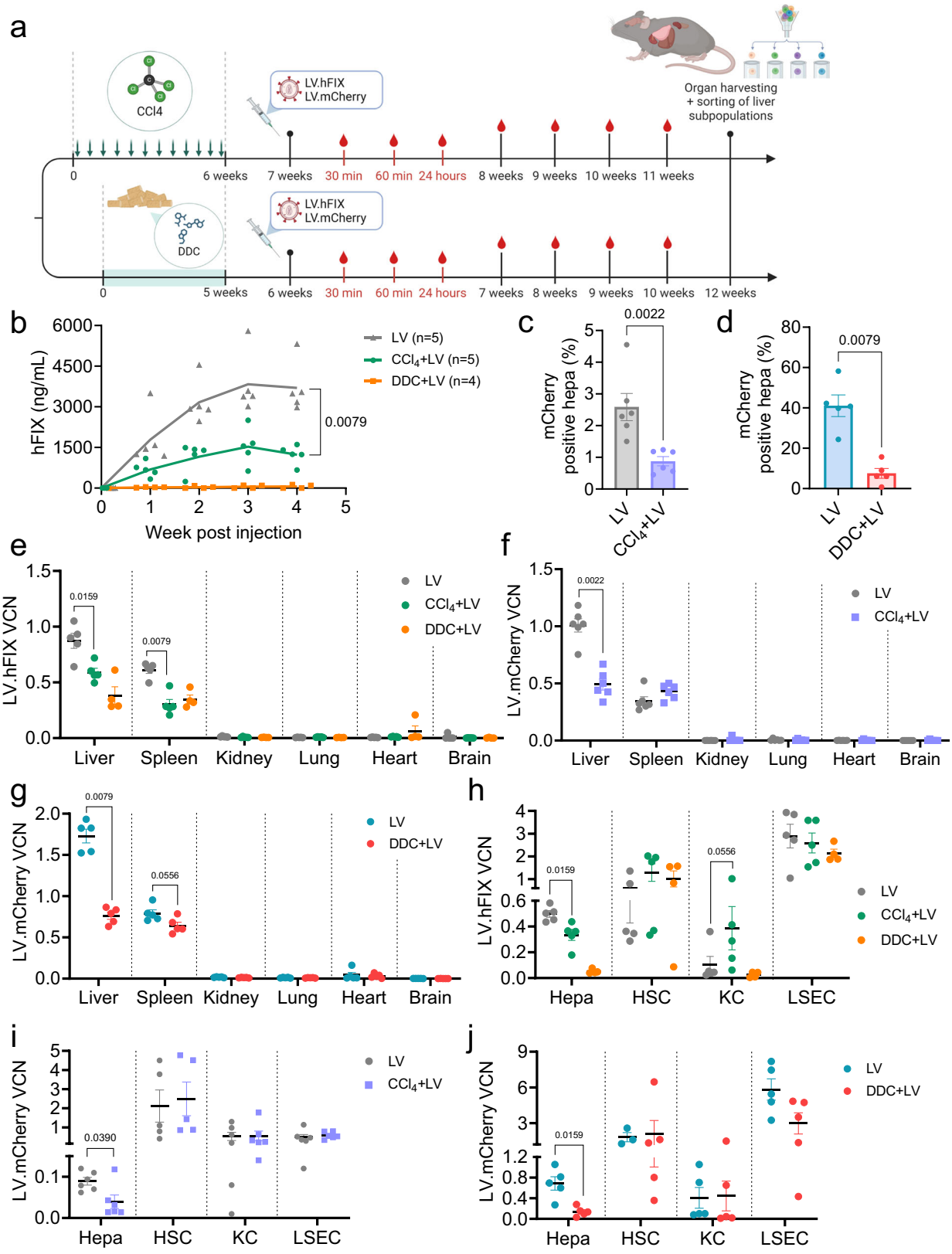

Milder fibrosis, induced by CCl_4 or DDC, reduces LV and AAV vector transduction efficiency

To investigate LV- and AAV-vector-mediated gene transfer in the presence of milder fibrosis, we shortened the exposure time to CCl_4 or DDC, thus reducing the extent of tissue damage. We administered WT mice with the toxic compounds for 3 weeks. During treatments, we confirmed the induction of liver damage by showing serum ALT and AST elevation (>1500 U/L for DDC and >3000 U/L for CCl_4; Supplementary Fig. 5a, b). We then analyzed the state of liver fibrosis at the end of the toxic treatments by histopathology. We observed mild pericentral fibrosis in the CCl_4 model and moderate periportal fibrosis induced by the DDC diet (Fig. 4a, b and Supplementary Tables 1 and 2),

Fig. 3 | Liver fibrosis impacts LV transduction of hepatocytes without major alteration of LV biodistribution. a Experimental design scheme (green arrows and bar indicate CCl_4 administration or DDC diet, respectively) created with BioRender (https://BioRender.com/m06f740). LV.hFIX 5×10^{10} TU/kg. LV.mCherry in CCl_4 experiment 1.5×10^{10} TU/kg, in DDC experiment 4×10^{10} TU/kg. **b** Individual values with mean of hFIX concentration. (Mann–Whitney test at the last time point). Gray, green, and orange symbols indicate mice treated with LV ($n = 5$), with CCl_4 and LV ($n = 5$), or with DDC and LV ($n = 4$), respectively. **c**, **d** Individual values and mean ± SEM of percentage (%) of mCherry-positive hepatocytes (hepa; Mann–Whitney test). **c** Gray and purple symbols indicate mice treated with LV ($n = 6$) or with CCl4 and LV ($n = 6$), respectively. **d** Light blue and red symbols indicate mice treated with LV ($n = 5$) or DDC and LV ($n = 5$), respectively. **e** Individual values and mean ± SEM of VCN in indicated organs of mice administered with LV.hFIX (Mann–Whitney test). Gray, green, and orange symbols indicate mice treated with LV ($n = 5$), with CCl_4 and LV ($n = 5$), or with DDC and LV ($n = 4$), respectively. **f**, **g** Individual values and mean ± SEM of VCN in indicated organs of mice administered with LV.mCherry (Mann–Whitney test). **f** Gray and purple symbols indicate mice treated with LV ($n = 6$) or with CCl4 and LV ($n = 6$), respectively. **g** light blue and red symbols indicate mice treated with LV ($n = 5$) or DDC and LV ($n = 5$), respectively. **h** Individual values and mean ± SEM of VCN in indicated liver cells of mice administered with LV.hFIX (Mann–Whitney test). Gray, green, and orange symbols indicate mice treated with LV ($n = 5$), with CCl_4 and LV ($n = 5$), or with DDC and LV ($n = 4$), respectively. **i**, **j** Individual values and mean ± SEM of VCN in indicated liver cells of mice administered with LV.mCherry (Mann–Whitney test). **i** gray and purple symbols indicate mice treated with LV ($n = 6$) or with CCl4 and LV ($n = 6$), respectively. **j** light blue, and red symbols indicate mice treated with LV ($n = 5$) or DDC and LV ($n = 5$), respectively. Source data are provided as a Source Data file.

displaying similar inflammatory cell infiltrate as described above (see Figs. 1a and 2a). One week after the last CCl_4 administration or interruption of the DDC diet, we injected LV.mCherry into CCl_4-treated, DDC-treated, or control animals (Fig. 4c). On the other hand, we administered AAV.mCherry only to mice treated with DDC (Fig. 4c), since we did not observe a reduction of AAV-vector transduction in the presence of CCl_4-induced liver fibrosis (see Fig. 1e, f). We observed significant 1.9-fold and 3.2-fold reduction of mCherry-positive liver area in CCl_4– and DDC-treated mice, respectively (Fig. 4d and Supplementary Fig. 5c) paralleled by a reduction of liver VCN (Supplementary Fig. 5d). Concerning AAV-treated mice, we found a significantly 2-fold lower mCherry-positive liver area in DDC-treated mice compared to controls of both sexes (Fig. 4e, f and Supplementary Fig. 5e). Consistently with the reduced transgene expression, we found a significant 2-fold reduction in AAV VCN in the liver, as well (Supplementary Fig. 5f, g). These data show that the mild hepatic damage induced by CCl_4 or DDC treatments negatively influenced both LV and AAV vector transduction, as the marked damage induced in the experimental settings mentioned above (see Figs. 1 and 2).

Liver fibrosis due to *Abcb11* deficiency slightly reduces LV and AAV vector transduction

Next, we assessed the impact of liver fibrosis on viral vector transduction in genetic models. We first characterized the state of the liver of 6-month-old *Abcb11*$^{-/-}$ mice or WT age-matched controls by histopathology and evaluation of serum ALP. In *Abcb11*$^{-/-}$, we observed a significant elevation of ALP (>300 U/L; Supplementary Fig. 6a), ductular proliferation, mild periportal fibrosis, and minimal inflammatory cell infiltrate (Fig. 5a, b and Supplementary Table 3). None of these alterations were in control mice (Supplementary Table 3). We administered *Abcb11*$^{-/-}$ or WT control mice with LV.mCherry or AAV.mCherry and collected livers 2 weeks post vectors injection. In LV-treated *Abcb11*$^{-/-}$ mice, we observed a 1.9-fold decrease in the mCherry-positive liver area compared to controls (Fig. 5c and Supplementary Fig. 6b), paralleled by a similar LV VCN in the liver among the two groups (Supplementary Fig. 6c). In the livers of *Abcb11*$^{-/-}$ mice treated with AAV.mCherry, we detected a 1.3-fold reduction in mCherry-positive tissue area compared to *Abcb11*$^{+/+}$ mice (Fig. 5d and Supplementary Fig. 6d), accompanied by a decrease in AAV VCN in the liver (Supplementary Fig. 6e). These data highlight that the mild periportal fibrosis present in 6-month-old *Abcb11*$^{-/-}$ mice has only a minor negative impact on both LV and AAV vector-mediated gene transfer.

LV and AAV vector transduction is not significantly impaired in *Agl*$^{-/-}$ mice

We next took advantage of *Agl*$^{-/-}$ mice, a model of GSDIII previously shown to present with a minimal fibrotic state when adults[20]. We performed histopathology analysis to better characterize the liver fibrosis of 9-month-old *Agl*$^{-/-}$ mice ($n = 3$) or *Ag*$^{+/+}$ age-matched controls ($n = 2$). We detected minimal periportal fibrosis with mostly incomplete bridging septa and pseudo-nodules, while we did not detect alterations in control mice (Fig. 5e). We injected 9-month-old *Agl*$^{-/-}$ or age-matched control mice with LV.mCherry or AAV.mCherry, and we collected livers 2 weeks post vector administration. In both LV and AAV vector-treated animals, we did not observe significant differences in mCherry-positive liver area (Fig. 5f, g and Supplementary Fig. 6f, g) or liver VCN (Supplementary Fig. 6h, i). These data suggest that the minimal periportal liver fibrosis in *Agl*$^{-/-}$ mice does not substantially impact gene transfer to hepatocytes.

Liver fibrosis modifies the distribution of gene transfer within the liver lobule

To study the impact of liver fibrosis on gene transfer distribution across different liver lobule zones (zonation), we analyzed the liver samples from the experiments described above, i.e., the CCl_4 and DDC severe models (see Figs. 1 and 2), *Abcb11*$^{-/-}$ and *Agl*$^{-/-}$ mice (see Fig. 5). We performed immunofluorescence staining to mark the periportal zone with cytokeratin 7 (CK7), expressed by cholangiocytes, and the pericentral zone with glutamine synthetase (GS), expressed only by pericentral hepatocytes[25]. We then analyzed the mCherry-positive area within the periportal or pericentral area and calculated the fold between them to assess the gene transfer distribution (Fig. 6a, b). LV in control mice showed a preference for transduction in the periportal area (Fig. 6c), as previously shown by our group[26]. Interestingly, the periportal transduction bias was significantly reduced in all fibrosis models tested. Indeed, it almost disappeared in the presence of DDC-induced fibrosis, while in *Abcb11*$^{-/-}$ and *Agl*$^{-/-}$ mice, the transduction became more pericentral (Fig. 6c). By analyzing the mCherry-positive area in the two zones in each mouse, we detected a decrease only in the periportal and not in the pericentral transduction with CCl_4-induced fibrosis (Supplementary Fig. 7a). With DDC-induced fibrosis both periportal and pericentral transduction were reduced, but with a greater extent in the periportal zone (Supplementary Fig. 7a). On the contrary, in *Abcb11*$^{-/-}$ and *Agl*$^{-/-}$ mice, periportal transduction was reduced but pericentral transduction was increased (Supplementary Fig. 7a). AAV vector serotype 8 used in this work showed pericentral transduction preference in control mice (Fig. 6d), as already described[27]. The CCl_4 and DDC-induced liver fibrosis did not impact the AAV vector transduction bias (Fig. 6d). The pericentral transduction bias appeared to increase In *Abcb11*$^{-/-}$ mice, while it was decreased in *Agl*$^{-/-}$ mice (Fig. 6d). Regarding the mCherry positive area, DDC treatment induced an overall decrease in transduction in both zones, in *Abcb11*$^{-/-}$ mice only the periportal transduction was decreased, and in *Agl*$^{-/-}$ mice the pericentral transduction was more reduced than the periportal transduction (Supplementary Fig. 7b). These data suggest an overall modification of the zonation of gene transfer that was dependent on both the delivery vector and the liver fibrosis model.

https://doi.org/10.1038/s41467-025-57383-8

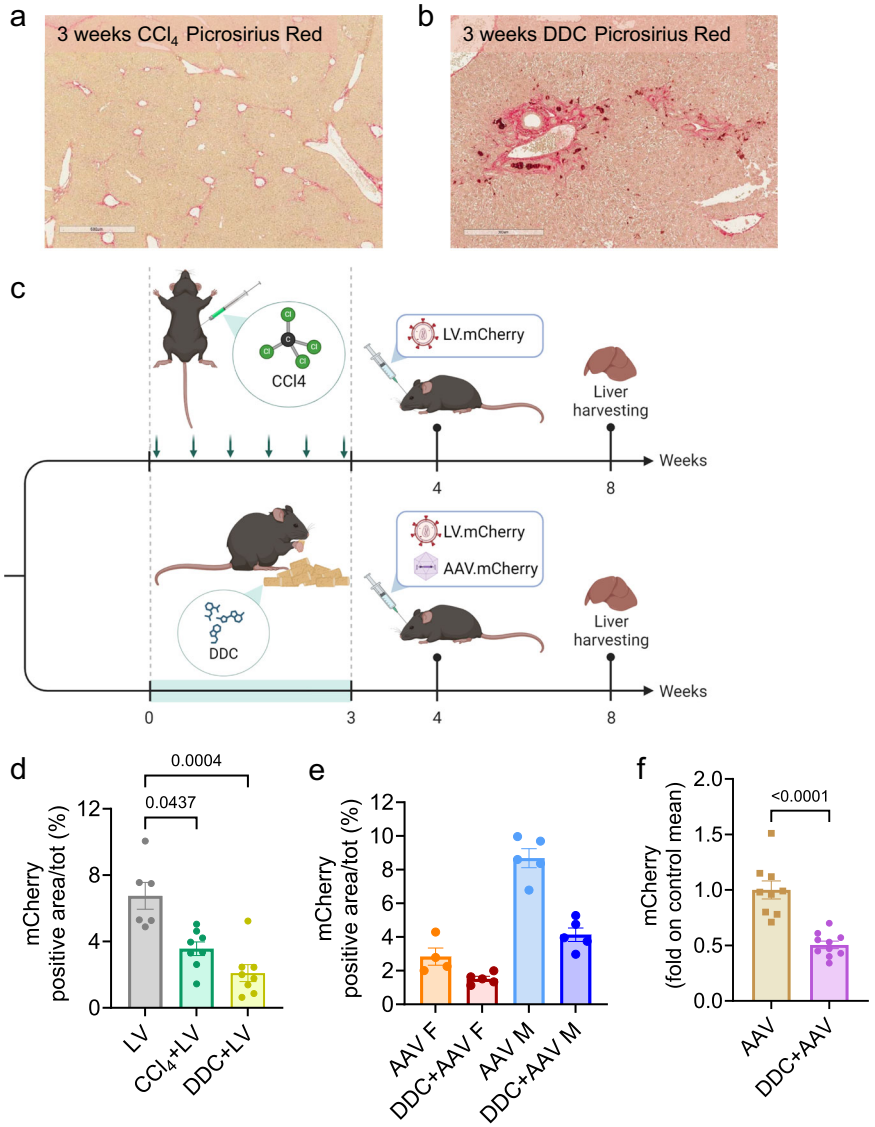

Fig. 4 | Milder fibrosis, induced by CCl_4 or DDC, reduces LV and AAV vector transduction efficiency. a, **b** Representative histological images of liver sections from mice treated with CCl_4 ($n = 6$) or fed with a DDC-supplemented diet ($n = 8$) for 3 weeks (**a**, bar = 600 μm, **b** bar = 300 μm). Picrosirius red staining. **c** Schematics of experimental design with timeline (green arrows indicate CCl_4 administrations, green bar indicates DDC diet). LV.mCherry 1×10^{10} TU/kg. AAV.mCherry 1×10^{11} vg/kg. Created with BioRender (https://BioRender.com/t54x010). **d**, **e** Individual values and mean ± SEM of percentage (%) of the mCherry-positive liver area expressed over the total area analyzed (**d** Kruskal–Wallis test). **d** Gray symbols indicate mice treated with LV only ($n = 6$), green symbols indicate mice treated with CCl_4 and LV ($n = 8$), and yellow symbols indicate mice treated with DDC and LV ($n = 8$). **e** orange symbols indicate female mice treated with AAV only ($n = 4$), red symbols indicate female mice treated with DDC and LV ($n = 5$), light blue symbols indicate male mice treated with AAV only ($n = 5$), blue symbols indicate male mice treated with DDC and LV ($n = 5$). **f** Individual values with mean ± SEM of mCherry-positive liver area percentage (%) expressed as fold on the mean of each respective control group (Mann–Whitney test; row data displayed in (**e**)). Brown symbols indicate mice treated with AAV only ($n = 9$), and purple symbols indicate mice treated with DDC and AAV ($n = 10$). Source data are provided as a Source Data file.

Discussion

Here, we perform a detailed characterization of the impact of liver fibrosis on in vivo gene transfer to hepatocytes in four different mouse models, two chemically induced and two genetic, by both LV and AAV vectors, two widely used viral vector platforms. Although chemical fibrosis models are relatively artificial, they are extensively adopted to mimic the more common fibrosis types found in human conditions. In particular, the CCl_4 model resembles fibrosis due to toxic damage and viral hepatitis, while the DDC model recapitulates fibrosis due to cholestatic disease[4]. We report that hepatocytes within fibrotic livers are generally transduced with reduced efficiency. However, the outcome varied according to the vector used and the state of the tissue at the time of systemic vector administration. Specifically, CCl_4-induced toxic pericentral fibrosis, either scored as moderate or mild, negatively affected LV transduction. On the contrary, this type of fibrosis did not significantly alter AAV vector transduction. Instead, DDC-induced biliary fibrosis impaired LV- and AAV-vector-mediated gene transfer, both in the presence of moderate and marked periportal damage. In line with this finding, we observed a slight reduction of LV and AAV vector transduction in *Abcb11*$^{-/-}$ mice, which display mild biliary fibrosis. However, the decrease in gene transfer was less pronounced in 6-month-old *Abcb11*$^{-/-}$ mice than in DDC-fed mice. By contrast, the minimal periportal liver fibrosis in 9-month-old *Agt*$^{-/-}$ mice did not significantly affect LV or AAV-vector transduction. These data suggest that the type and extent of damage determine the impact on gene transfer efficiency, in accordance with the few previous reports on

https://doi.org/10.1038/s41467-025-57383-8

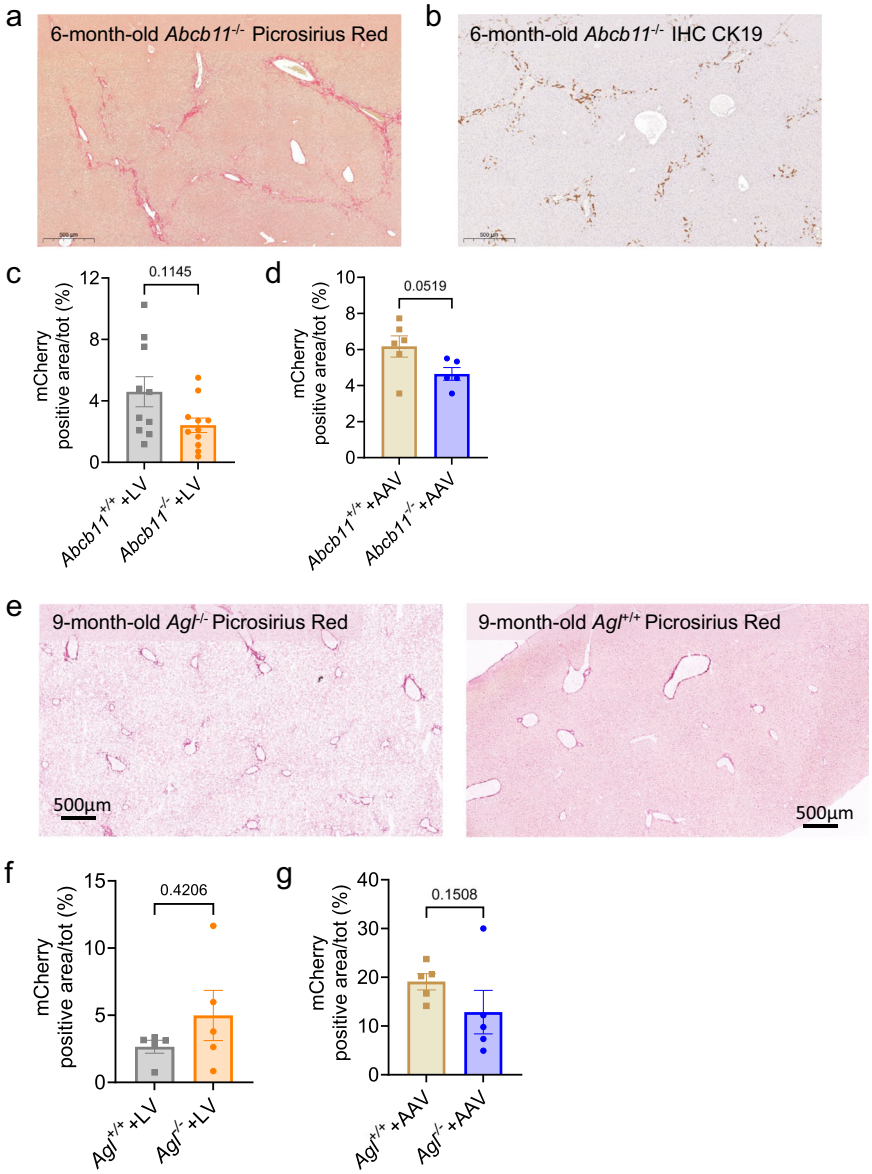

Fig. 5 | Liver fibrosis due to *Abcb11* deficiency slightly reduces LV and AAV vector transduction, while LV and AAV vector transduction is not significantly impaired in *Agl*$^{-/-}$ mice. a, **b** Representative histological images of liver sections from 6-month-old *Abcb11*$^{-/-}$ mice (bar = 500 µm). Picrosirius red staining (**a**) and IHC CK19 (**b**). **c**, **d** Individual values and mean ± SEM of percentage (%) of the mCherry-positive liver area expressed over the total area analyzed (two-tailed Mann–Whitney test). LV.mCherry 3.5×10^{10} TU/kg. AAV.mCherry 1×10^{11} vg/kg. **c** Gray symbols indicate *Abcb11*$^{+/+}$ mice treated with LV ($n = 10$), and orange symbols indicate *Abcb1*$^{-/-}$ mice treated with LV ($n = 11$). **d** brown symbols indicate *Abcb11*$^{+/+}$ mice treated with AAV ($n = 6$), and blue symbols indicate *Abcb1*$^{-/-}$ mice treated with AAV ($n = 5$). **e** Representative histological images of liver sections from 9-month-old *Agl*$^{-/-}$ (left) and age-matched *Agl*$^{+/+}$ male mice (right) (bar = 500 µm). Picrosirius red staining. **f**, **g** Individual values and mean ± SEM of percentage (%) of the mCherry-positive liver area expressed over the total area analyzed (Mann–Whitney test). LV.mCherry 5×10^{10} TU/kg. AAV.mCherry 1×10^{11} vg/kg. **f** Gray symbols indicate *Agl*$^{+/+}$ mice treated with LV ($n = 5$), and orange symbols indicate *Agl*$^{-/-}$ mice treated with LV ($n = 5$). **g** Brown symbols indicate *Agl*$^{+/+}$ mice treated with AAV ($n = 5$), and blue symbols indicate *Agl*$^{-/-}$ mice treated with AAV ($n = 5$). Source data are provided as a Source Data file.

AAV-vector-mediated liver transduction showing fibrosis-model-dependent outcomes[28,29].

Of note, when using AAV vectors, the reduction of hepatocyte-derived transgene output was always paralleled by a reduction of AAV VCN in the liver since AAV vector serotype 8 has specific tropism for hepatocytes. On the other hand, when using LV, the decrease in gene transfer efficiency was not always mirrored by a lower LV VCN in the liver. This finding is expected since VSV.G-pseudotyped LV also transduces liver non-parenchymal cells. Therefore, VCN in the total liver did not directly reflect the transduction of hepatocytes, as we have previously shown[12]. Indeed, when we measured VCN in purified hepatocytes from the liver of experimental mice, we reported a direct correlation between transgene output and hepatocyte transduction by LV. These data suggest that the reduction of transgene output in the presence of liver damage is primarily due to decreased hepatocyte transduction rather than transgene expression.

The different gene transfer outcomes observed in our fibrosis models may also depend on the underlying pathogenic mechanisms and specific cell responses. Primarily, chronic activation of the fibrogenic pathway leads to an altered tissue structure due to changes in the composition and distribution of the extracellular matrix throughout the liver lobules. The deposition of collagen, alterations of structures like endothelial *fenestrae*, and induction of neo-angiogenesis result in higher pressure on the liver microvasculature, causing portal

https://doi.org/10.1038/s41467-025-57383-8

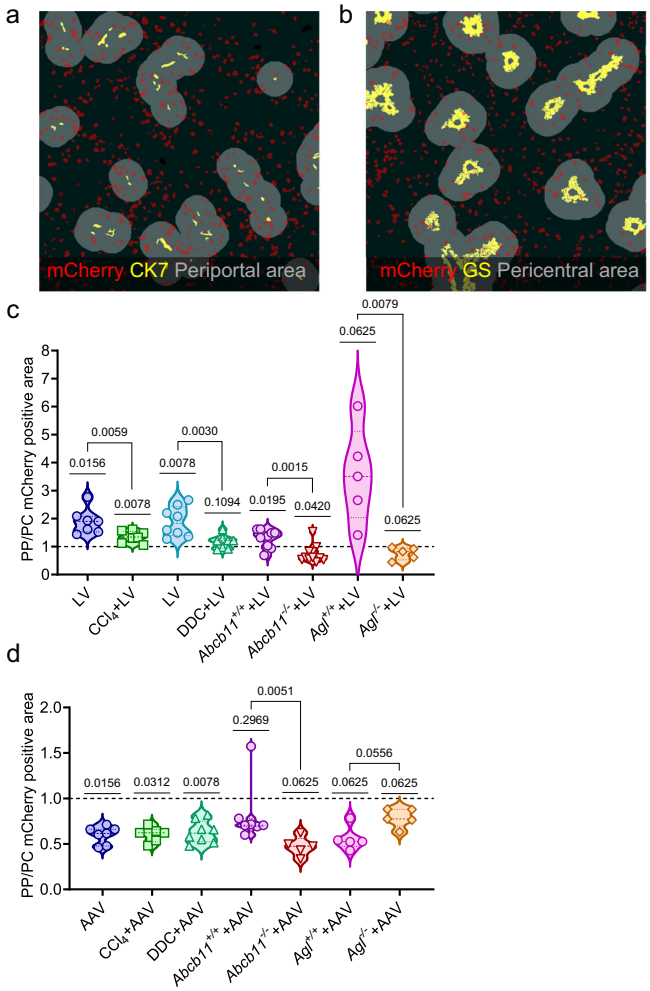

Fig. 6 | Liver fibrosis modifies the distribution of gene transfer within the liver lobule. a, **b** Representative images of zonation analysis, based on immunofluorescence staining of liver sections from control mice administered with LV.mCherry. Gray circles indicate the analyzed periportal (**a**) or pericentral (**b**) areas. **a** Anti-mCherry antibody (red), anti-CK7 antibody (yellow), and periportal area (gray). **b** Anti-mCherry antibody (red), anti-GS antibody (yellow), and pericentral area (gray). **c**, **d** Violin plot with individual values, median, and quartiles of the fold between periportal (PP) over pericentral (PC) mCherry-positive liver area of mice treated with LV.mCherry (**c**) or AAV.mCherry (**d**) (Wilcoxon signed-rank test against 1, Kruskal–Wallis test, or Mann–Whitney test between test and control groups). The dotted line represents fold = 1. Row data are displayed in Supplementary Fig. 7. Source data are provided as a Source Data file.

hypertension and changes in overall blood flow. In turn, this leads to abnormal circulation of substances between blood vessels and the liver parenchyma[1]. All these changes could hamper the physical accessibility of the viral vectors to hepatocytes when administered systemically. Notably, LV and AAV vectors have different sizes, approximately 120 nm and 25 nm, respectively[30]. Therefore, a physical barrier may inhibit more strongly LV rather than AAV vector delivery to hepatocytes. However, our finding that periportal liver fibrosis inhibited both LV and AAV vector gene transfer supports that other mechanisms contribute to transduction impairment. Interestingly, we observed an overall change in the zonation of gene transfer in the presence of liver damage, and even when transduction was not reduced per se. Regarding LV, the periportal transduction bias was reduced in the case of periportal fibrosis (DDC-induced, *Abcb11*$^{-/-}$, *Agl*$^{-/-}$). This may be due to the collagen deposition restricting access to periportal hepatocytes. However, also in the context of CCl_4-induced pericentral fibrosis, the periportal LV transduction was reduced. This observation may be explained by an overall alteration of the liver metabolism following CCl_4 chronic administration, which reduced the transduction of periportal hepatocytes, even if they were not near the area of collagen deposition. The AAV serotype 8 pericentral bias of transduction was maintained in the presence of CCl_4 and DDC-induced fibrosis. The DDC diet impaired transduction overall, independently on the lobule area. On the other hand, in *Abcb11*$^{-/-}$ mice, the pericentral bias appeared to increase, while in *Agl*$^{-/-}$ mice, it decreased. The overall changes in zonation of transduction in the tested models may be due to alteration of the metabolic state of the liver rather than to a simple physical barrier caused by extracellular matrix deposition. In this regard, an altered metabolic state of hepatocytes and other liver cells may also affect the expression of vector receptors and impact other post-entry steps of the vector transduction process, such as capsid trafficking, nuclear import, and nucleic acid synthesis. Moreover, the presence of inflammatory cell infiltrates, as observed in most fibrosis models, may cause an increase in phagocytosis and reinforce cellular anti-viral defenses, thus leading to reduced transduction. We addressed whether LV gene transfer into hepatocytes was accompanied by increased vector clearance or skewed vector distribution to other liver cell types or tissues. However, in our experimental settings, we did not detect any change in LV clearance from the blood and no major skewing of LV transduction away from the liver or hepatocytes to other major organs or liver non-parenchymal cells. These observations might be explained by the inflammatory state of the liver impairing hepatocyte transduction without an evident increase in VCN in other cell types and tissues. Overall, our study highlights that inhibition of vector transduction is likely caused by multifactorial mechanisms driven by the liver damage occurring in the different models that we investigated.

Importantly, we never observed a complete abrogation of transduction and transgene expression in any of the pathological conditions evaluated in this study, suggesting that gene transfer to hepatocytes can still be achieved, even if hepatic fibrosis is present at the time of vector administration. However, our findings indicate that the presence of pre-existing liver fibrosis needs to be carefully considered when developing and administering liver-directed gene therapy. Specifically, the vector dose may need to be increased to achieve the same therapeutic efficacy in patients with fibrotic liver compared to those with a non-fibrotic liver. Moreover, the time of vector administration should be anticipated as much as possible to avoid the progression of liver disease, and patient populations should be selected according to the presence and stage of damage. Furthermore, since hepatic fibrosis may trigger hepatocyte proliferation, AAV vector-mediated transgene expression may progressively decrease because of dilution of AAV vector episomes[31]. The impact of hepatic fibrosis on gene transfer may also vary according to different vector envelopes/serotypes. Thus, the vector platform and design need to be wisely selected based on the target disease and underlying liver damage. Since viral vectors can be used as delivery tools for genome editing machinery[32], our work is also informative for the design of precise genetic modification strategies.

The limitations of this work include the use of chemically induced models that, even if extensively exploited, only mimic some of the pathological mechanisms found in human conditions. Here, we did not specifically investigate the fibrosis occurring in alcoholic or metabolic-associated steatohepatitis. In addition, our work involves mouse models that may not be fully predictive of human outcomes. Moreover, further investigation will be required to better understand the molecular mechanisms by which liver fibrosis impacts gene transfer and to devise potential strategies to overcome them.

Overall, the study reported here sheds light on a previously unexplored yet critical aspect of liver-directed gene therapy and has several implications for future developments and applications of liver-directed gene transfer and editing.

Methods

Generation of LV and AAV vector plasmids

We used transfer plasmids for LV productions (pCCLsin.cPPT.ET.co-hFIXR338L.142T.Mwpre.142T and pCCLsin.cPPT.ET.mCherry.W-pre.4x142-3PT) obtained by standard cloning techniques from previously described backbones[12]. For AAV vector production, we used plasmids with hFIX or mCherry expression cassette containing the apolipoprotein E (ApoE) and human alpha1-antitrypsin (hAAT) promoter, the hFIX cDNA, the hFIX intron located just after exon 1 and a bovine growth hormone (bGH) poly-A, as previously described in ref. 22.

LV production and titration

We employed human embryonic kidney (HEK) 293T cells for vector production and titration. We maintained HEK293T in Iscove's modified Dulbecco's medium (IMDM, Corning) supplemented with 10% Cytiva HyClone™ FetalClone™ II Serum (U.S.) (Euroclone) and penicillin/streptomycin 100 international units (IU)/mL (Lonza). We detached cells using PBS 0.05% trypsin, and 4 mM EDTA solution. We maintained cells in a humidified incubator at 37 °C 5% CO_2. We produced third-generation self-inactivating (SIN) LV by calcium phosphate transfection of HEK 293T cells with a mix of transfer plasmid and packaging plasmids, as previously described in ref. 9. We filtered LV-containing supernatant with a 0.22 µm filter (Millipore) and concentrated around 4-fold with Vivaflow 200 Tangential Flow Filtration Cassette 100 kDa (Sartorius), according to the manufacturer's instructions. Subsequently, we ultracentrifuged the supernatant in polyallomer tubes (Beckman Optima XL-100K Ultracentrifuge). We concentrated the final LV around 500-fold by resuspending the pellet in an appropriate volume of phosphate saline buffer (PBS, Corning). We prepared LV aliquots, which were stored at −80 °C. We measured the LV infectious titer as previously described in ref. 9. We extracted genomic DNA (gDNA) using Maxwell RSC Cultured Cells DNA Kit (AS1620, Promega) following the manufacturer's instructions. We determined vector copies per diploid genome (vector copy number, VCN) by digital droplet PCR (ddPCR), as previously described in ref. 9.

AAV vector production and titration

We produced AAV vectors using an adenovirus-free transient transfection method and performed purification using a chromatographic method as described earlier in ref. 23. We determined titers of the AAV vector stocks using a real-time qPCR using primers on the hAAT promoter (Forward: 5′ GGC GGG CGA CTC AGA TC 3′ and Reverse: 5′ GGG AGG CTG CTG GTG AAT ATT 3′).

Mice experiments

We carried out all animal experiments under good animal practices following Italian and European legislation on animal care and experimentation (2010/63/EU) and approved by the Italian Ministry of Health ethical committee (protocol number 6EEAF.341). In the experiments we used C57BL/6, *Abcb11*$^{-/-}$ and *Agl*$^{-/-}$ mice. We purchased C57BL/6 mice from Charles River Laboratories. We purchased *Abcb11*$^{-/-}$ mice from The Jackson Laboratory (strain #004125). The *Agl* knockout (*Agl*$^{-/-}$) mice were developed in the frame of the International Mouse Phenotyping Consortium (IMPC). Mice were generated in a pure C57BL/6J background by replacing exons 6–10 of the *Agl* gene with a neomycin-expressing cassette. Mice were bred into a mixed BALB/c background. All mice were maintained in specific pathogen-free conditions and fed *ad libitum* with VRF1 (P) by Special Diet Services. To genotype *Abcb11*$^{-/-}$ mice, we extracted gDNA from tissue biopsies obtained by ear clipping procedure. We resuspended each biopsy in 25 µL of QuickExtract DNA extraction solution (Biosearch technologies), incubated at 65 °C for 6 min, and then at 98 °C for 2 min. We then performed PCR genotyping, as detailed on The Jackson Laboratory website, strain #004125. We performed genotyping of *Agl*$^{-/-}$ mice as previously described in ref. 21. In CCl_4 experiments, we intraperitoneally injected 6-week-old C57BL/6 mice with 0.6 µL/g of body weight of CCl_4 (289116, Sigma-Aldrich) that was diluted in corn oil to reach a final volume of 50 µL, or with 50 µL of corn oil alone as controls. We administered the treatment for a period of 3 or 6 weeks, depending on the experiment. In DDC experiments, we fed 6-week-old C57BL/6 mice with a standard diet supplemented with 0.1% (*w*/*w*) of DDC (137030, Sigma-Aldrich) for a period of 3 weeks or 5 weeks, depending on the experiment. In these experiments, we delivered LV or AAV vectors by i.v. retro-orbital administration. We always included age and sex-matched controls injected in parallel with the same doses of LV or AAV vectors. We collected blood samples from the retro-orbital plexus with or without 0.38% sodium citrate anticoagulant buffer pH 7.4 for plasma or serum preparation, respectively. In experiments with *Abcb11*$^{-/-}$ mice, we delivered LV or AAV vectors to 6-month-old male and female mice by i.v. retro-orbital administration, including *Abcb11*$^{+/+}$ mice as controls. In experiments with *Agl*$^{-/-}$ mice, we administered LV or AAV vectors i.v. via the tail vein to 9-month-old male *Agl*$^{-/-}$ mice and *Agl*$^{+/+}$ littermates. We euthanized the mice by cervical dislocation. The experiments were not blinded to the sample code. We processed samples blind to the sample code only for histopathological analysis up to the stage of data analysis. We reported the experiments involving animals following the ARRIVE guidelines.

Determination of hepatic clinical chemistry

We used commercially available ALT (Instrumentation Laboratory, #0018257440), AST (Instrumentation Laboratory, #0018257540), and ALP (Instrumentation Laboratory, #18259740) controls for the quantitative determination of the serum ALT, AST, and ALP concentration with an International Federation of Clinical Chemistry and Laboratory Medicine–optimized kinetic ultraviolet (UV) method in an ILab650 chemical analyzer (Instrumentation Laboratory). We analyzed SeraChem Control Level 1 and Level 2 (#0018162412 and #0018162512) as quality controls.

Liver histopathology analysis

We harvested livers from mice and fixed them in buffered 4% buffered formalin by immersion. We embedded livers in paraffin, and then we sectioned and mounted them on glass slides. We stained 2.5-µm paraffin sections with hematoxylin-eosin and Picrosirius Red for histopathological evaluation and analysis of collagen deposition. We captured images from digitalized slides scanned using Aperio Scanscope (Leica) and Pannoramic Midi (3D Histech). For the cytokeratin 19 immunohistochemistry assay (IHC CK19), we used the rabbit monoclonal antibody anti-CK19 clone EP1580Y (Abcam), diluted 1:1000, and incubated 1 h at RT.

Enzyme-linked immunosorbent assay (ELISA)

To determine hFIX antigen concentration in mouse plasma, we used a paired antibody set (FIX-EIA, Affinity Biologicals). We coated plates with 100 µL of capture antibody (FIX-EIA-C, 1:200 diluted in 50 mM carbonate pH 9.6) and incubated them overnight at 4 °C. We washed plates three times with PBS 0.05% (*v*/*v*) Tween-20 and incubated them with 100 µL of samples diluted in PBS 0.05%, Tween 1%, bovine serum albumin (BSA) or standard controls for 2 h at room temperature (RT), in technical duplicates. We washed plates three times and we added an HRP-conjugated detection antibody (FIX-EIA-D, 1:200 diluted in PBS 0.05% Tween 1% BSA), which was incubated for 1.5 h at RT. After three washes, we added 100 µL of 3,3′, 5,5′-Tetrametil-benzidine substrate for 5 min and stopped the reaction with 50 µL of hydrochloric acid 1 M. We read plates at 450 nm using a Multiskan GO microplate reader (Thermo Fisher Scientific).

Liver immunofluorescence imaging

We fixed mouse livers in PBS 4% paraformaldehyde (PFA) for 4 h, then moved them to 30% sucrose 0.02% sodium azide for at least 24 h. We embedded livers in OCT (optimal cutting temperature) compound

(Killik, Bio Optica) and prepared 10 µm-thick slices using a cryostat (Histo-line MC5050). We placed slices on Superfrost Plus microscope slides (Epredia) and stored them at −80 °C. For the staining, we thawed the slides at room temperature for at least 2 h, then washed them three times in PBS 0.1% X-Triton. We blocked non-specific bindings incubating slides with PBS 0.1% X-Triton 5% FBS 1% BSA for 1 h at room temperature in a humid chamber. We substituted the blocking solution with a primary antibody mix diluted in the blocking solution, which was incubated overnight at 4 °C in a humid chamber. After three washes with PBS 0.1% X-Triton, we added a secondary antibody mix diluted in blocking solution with Hoechst 33342 (1:2000, H3570, Life technologies), which was incubated for 1 h at room temperature in a humid chamber. We washed the slides in PBS and added Fluoromount-G (Invitrogen) to mount the coverslip. We used the following antibodies:

Antigen	Species	Fluorochrome	Clone	Company (code)	Dilution
mCherry	Chicken	–	Polyclonal	Abcam (ab205402)	1:1000
CK7	Rabbit	–	Polyclonal	Abcam (ab181598)	1:250
GS	Rabbit	–	Polyclonal	Novus Bio (NB110-4104)	1:5000
Chicken IgY	Goat	AF546	Polyclonal	Invitrogen (A11040)	1:1000
Rabbit IgG	Donkey	AF647	Polyclonal	Invitrogen (A31573)	1:1000

We acquired images using the confocal microscope Mavig Rs-G4 (RSG4 software) at 20× magnification and analyzed them with MATLAB software (9.13.0.2126072 (R2022b) Update 3) after manually excluding unwanted areas like fringed borders. We exploited a custom MATLAB script that quantified the mCherry-positive tissue area, automatically calculating the threshold for each image based on the signal intensity (Supplementary Code 1). The script measured the total liver area by saturating the signal from the whole tissue. Periportal and pericentral areas were identified by marking tissue area within a fixed distance from CK7- or GS-positive area using MATLAB. CK7, GS areas, and hepatocytes were segmented from their respective fluorescent images by first filtering out background fluorescence and small-scale noise and then applying a threshold. An additional filter on the dimension ensures the discard of unreasonably small or large objects (<100 μm^2, outliers area distribution). The whole tissue is also segmented through a very low threshold detecting autofluorescence; unwanted areas like fringed borders are manually excluded. PP and PC regions are defined as morphological dilations of CK and GS segmented areas of the specified radii (225 µm) that follow within the tissue. We finally measured the fraction of hepatocyte area in the PP and PC regions using MATLAB (Supplementary Code 2).

VCN determination

In LV experiments, we extracted gDNA from 50 mg of liver tissue using Maxwell RSC Tissue DNA Kit (AS1610, Promega) following the manufacturer's instructions. In AAV vector experiments, we extracted gDNA from 50 mg of liver tissue using DNeasy Blood & Tissue Kit (69504, Qiagen) following the manufacturer's instructions. We determined LV VCN for LV titration, and AAV VCN by ddPCR using primers (hAAT Fw: 5′-GGCGGGCGACTCAGATC-3′, hAAT Rv: 5′-GGGAGGCT GCTGGTGAATATT-3′) and a probe (hAAT Pr: 5′-(FAM)- AGCCCC TGTTTGCTCCTCCGATAACTG-(TAMRA)-3′). For both LV and AAV VCN determination, we quantified mouse gDNA using primers (Sema Fw: 5′-ACCGATTCCAGATGATTGGC-3′; Sema Rv: 5′- TCCATATTAATGCA GTGCTTGC−3′) and probe (Sema Pr: 5′-(HEX)-AGAGGCCTGTCCTG CAGCTCATGG-(BHQ1)-3′) designed on Sema3a reference gene.

LV p24 measurement in serum

We measured LV p24 in the serum of mice using Simple Plex HIV-1 Gag p24 Cartridge (SPCKB-PS-000981, R&D systems) following the manufacturer's instructions. We diluted 1:1000 serum samples collected 30 min after injection, 1:100 serum samples collected 60 min after, and 1:10 serum samples collected at 24 h.

Sorting of liver subpopulations

To sort liver subpopulations, we followed a previously described protocol[12]. We digested mouse liver exploiting perfusion through the inferior vena cava of collagenase IV (Sigma). We created a cell suspension by passing the liver through a 100µm cell strainer (BD Biosciences). We centrifuged cells at 30 g, 25 g, and 20 g for 3 min sequentially, to separate hepatocytes (pelleted) from nPCs (in the supernatant). We stained hepatocytes by diluting in 200 µL of PBS the following antibodies:

Antigen	Fluorochrome	Clone	Company (code)	Volume
CD31	APC	MEC 13.3	BD Biosciences (551262)	3 µL
CD45	APC	30-F11	BD Biosciences (559864)	3 µL
FC block		2.4G2	BD Biosciences (553142)	5 µL

After 20 min of incubation at room temperature, we washed them with HBSS (Hank's balanced salt solution, Gibco) 1% HEPES (4-(2-hydroxyethyl)-1-piperazineethanesulfonic acid). We sorted hepatocytes using MoFlo Astrios (Backman Coulter), selecting the APC-negative population and analyzing the percentage of mCherry-positive hepatocytes. We centrifuged nPCs in the supernatant for 10 min at 650 g. Then, we loaded cells in a Percol gradient of 30–60% and centrifuged for 15 min at 1800g. We collected the nPC interface and washed it twice with HBSS 1% HEPES. Firstly, we incubated nPCs for 15 min with 5 µL of FC Block, then we stained them with the following antibody mix, diluted in 200 µL of PBS:

Antigen	Fluorochrome	Clone	Company (code)	Volume
CD31	FITC	MEC 13.3	BD Biosciences (551262)	7 µL
CD45	BV786	104	BD Biosciences (563686)	7 µL
F4/80	PE	CI:A3-1	BD Biosciences (553142)	7 µL
CD45R/B220	PE-Cy5	RA3-6B2	BD Biosciences (553091)	7 µL
CD11c	PE-Cy7	N418	Invitrogen (25-0114-82)	7 µL

After 20 min of incubation at 4 °C, we washed them with HBSS 1% HEPES. We sorted KC, LSEC, and HSC, using BD FACSAria Fusion (BD Biosciences), according to surface marker expression or autofluorescence (gating strategy shown in Supplementary Fig. 4i).

Statistics and reproducibility

We presented data as individual values with mean ± standard error of the mean (SEM) or as individual values with mean. We performed statistical analyses using GraphPad Prism software (10.2.0.392) upon consulting with professional statisticians at the San Raffaele University

Center for Statistics in the Biomedical Sciences (CUSSB). We applied inferential techniques in the presence of adequate sample sizes ($n \geq 5$), otherwise we reported only descriptive statistics. We performed the two-tailed Mann–Whitney test when comparing two independent groups, or the Kruskal–Wallis test followed by post hoc analysis (Dunn's test for multiple comparisons against the reference control group along with Bonferroni's correction) for the comparison of more than two independent groups. Regarding experiments performed with AAV vectors, we represented the same data firstly by dividing male and female groups since their absolute values were different, then we performed the fold of each value on the mean of the respective controls to normalize the data and perform statistical analysis. Regarding the zonation analysis, we presented data as individual values with median and quartiles. To compare the median of our samples with the hypothetical value of 1, we performed the two-tailed Wilcoxon signed-rank test.

Reporting summary

Further information on research design is available in the Nature Portfolio Reporting Summary linked to this article.

Data availability

The authors declare that the main data supporting the findings of this study are available within the article and its Supplementary Information files. The LV, AAV, and reagents described in this manuscript are available to interested scientists upon signing an MTA with standard provisions. Contact person: Cantore Alessio (cantore.alessio@hsr.it), San Raffaele Telethon Institute for Gene Therapy, IRCCS San Raffaele Scientific Institute, Via Olgettina 58, Milan, Italy. Expected timeframe for response: ten working days. Source data are provided with this paper.

Code availability

The authors declare that the custom MATLAB scripts used to analyze immunofluorescence images are available within the Supplementary Information file.

References

1. Roehlen, N., Crouchet, E. & Baumert, T. F. Liver fibrosis: mechanistic concepts and therapeutic perspectives. *Cells* **9**, 875 (2020).
2. Scorza, M. et al. Genetic diseases that predispose to early liver cirrhosis. *Int J. Hepatol.* **2014**, 1–11 (2014).
3. Alam, S. & Lal, B. B. Recent updates on progressive familial intrahepatic cholestasis types 1, 2 and 3: Outcome and therapeutic strategies. *World J. Hepatol.* **14**, 98 (2022).
4. Parola, M. & Pinzani, M. Liver fibrosis: pathophysiology, pathogenetic targets and clinical issues. *Mol. Asp. Med.* **65**, 37–55 (2019).
5. Nathwani, A. C., McIntosh, J. & Sheridan, R. Liver gene therapy. *Hum. Gene Ther.* **33**, 879–888 (2022).
6. Ozelo, M. C. et al. Valoctocogene roxaparvovec gene therapy for hemophilia A. *N. Engl. J. Med.* **386**, 1013–1025 (2022).
7. Pipe, S. W. et al. Gene therapy with etranacogene dezaparvovec for hemophilia B. *N. Engl. J. Med.* **388**, 706–718 (2023).
8. Baruteau, J., Brunetti-Pierri, N. & Gissen, P. Liver-directed gene therapy for inherited metabolic diseases. *J. Inherit. Metab. Dis.* **47**, 9–21 (2024).
9. Milani, M. et al. Liver-directed lentiviral gene therapy corrects hemophilia A mice and achieves normal-range factor VIII activity in non-human primates. *Nat. Commun.* **13**, 2454 (2022).
10. Clar, J. et al. Hepatic lentiviral gene transfer prevents the long-term onset of hepatic tumours of glycogen storage disease type 1a in mice. *Hum. Mol. Genet.* **24**, 2287–2296 (2015).
11. Nicolas, C. T. et al. In vivo lentiviral vector gene therapy to cure hereditary tyrosinemia type 1 and prevent development of precancerous and cancerous lesions. *Nat. Commun.* **13**, 5012 (2022).
12. Milani, M. et al. Phagocytosis-shielded lentiviral vectors improve liver gene therapy in nonhuman primates. *Sci. Transl. Med.* **11**, eaav7325 (2019).
13. Philipp, C. The aging patient with hemophilia: complications, comorbidities, and management issues. *Hematology* **2010**, 191–196 (2010).
14. Mak, K. Y. et al. ACE2 therapy using adeno-associated viral vector inhibits liver fibrosis in mice. *Mol. Ther.* **23**, 1434–1443 (2015).
15. Bu, F. T. et al. Emerging therapeutic potential of adeno-associated virus-mediated gene therapy in liver fibrosis. *Mol. Ther. Methods Clin. Dev.* **26**, 191 (2022).
16. Jimenez, V. et al. Reversion of metabolic dysfunction-associated steatohepatitis by skeletal muscle-directed FGF21 gene therapy. *Mol. Ther.* **32**, 4285–4302 (2024).
17. Scholten, D., Trebicka, J., Liedtke, C. & Weiskirchen, R. The carbon tetrachloride model in mice. *Lab Anim.* **49**, 4–11 (2015).
18. Fickert, P. et al. A new xenobiotic-induced mouse model of sclerosing cholangitis and biliary fibrosis. *Am. J. Pathol.* **171**, 525–536 (2007).
19. Wang, R. et al. Targeted inactivation of sister of P-glycoprotein gene (spgp) in mice results in nonprogressive but persistent intrahepatic cholestasis. *Proc. Natl. Acad. Sci. USA* **98**, 2011 (2001).
20. Gardin, A. et al. A functional mini-GDE transgene corrects impairment in models of glycogen storage disease type III. *J. Clin. Invest.* **134**, e172018 (2024).
21. Vidal, P. et al. Rescue of GSDIII phenotype with gene transfer requires liver- and muscle-targeted GDE expression. *Mol. Ther.* **26**, 890–901 (2018).
22. Manno, C. S. et al. Successful transduction of liver in hemophilia by AAV-Factor IX and limitations imposed by the host immune response. *Nat. Med.* **12**, 342–347 (2006).
23. Collaud, F. et al. Preclinical development of an AAV8-hUGT1A1 vector for the treatment of Crigler–Najjar syndrome. *Mol. Ther. Methods Clin. Dev.* **12**, 157 (2019).
24. Davidoff, A. M., Ng, C. Y. C., Zhou, J., Spence, Y. & Nathwani, A. C. Sex significantly influences transduction of murine liver by recombinant adeno-associated viral vectors through an androgen-dependent pathway. *Blood* **102**, 480–488 (2003).
25. Paris, J. & Henderson, N. C. Liver zonation, revisited. *Hepatology* **76**, 1219–1230 (2022).
26. Starinieri, F. et al. Spatio-temporal dynamics of the liver shapes hepatocytes heterogeneity and impacts in vivo gene transfer and editing. *Res. Sq.* https://doi.org/10.21203/RS.3.RS-3138832/V1 (2023).
27. Bell, P. et al. Inverse zonation of hepatocyte transduction with AAV vectors between mice and non-human primates. *Mol. Genet. Metab.* **104**, 395–403 (2011).
28. Sobrevals, L. et al. AAV vectors transduce hepatocytes in vivo as efficiently in cirrhotic as in healthy rat livers. *Gene Ther.* **19**, 411–417 (2012).
29. Siew, S. M. et al. Prevention of cholestatic liver disease and reduced tumorigenicity in a murine model of PFIC type 3 using hybrid AAV-piggyBac gene therapy. *Hepatology* **70**, 2047–2061 (2019).
30. Li, X. et al. Viral vector-based gene therapy. *Int. J. Mol. Sci.* **24**, 7736 (2023).
31. Nakai, H. et al. Extrachromosomal recombinant adeno-associated virus vector genomes are primarily responsible for stable liver transduction in vivo. *J. Virol.* **75**, 6969–6976 (2001).
32. Simoni, C., Barbon, E., Muro, A. F. & Cantore, A. In vivo liver targeted genome editing as therapeutic approach: progresses and challenges. *Front. Genome Ed.* **6**, 1458037 (2024).

Acknowledgements

This work was mainly supported by the Fondazione Telethon SR-Tiget Core Grant (TTACC0422TT to A.C.). C.S. conducted this study in partial

fulfillment of her International Ph.D. Course in Molecular Medicine at San Raffaele University, Milan. J.N.'s work was supported by ARDAT (945473). We thank Andrea Annoni for his help with FACS to purify liver cell populations. We thank the ALEMBIC facility at the San Raffaele Scientific Institute for help with immune fluorescence analysis. We thank Micol Ravà at the Mouse Clinic facility for help with mouse clinical chemistry. We thank Chiara Brombin and Federica Cugnata at the San Raffaele University Center for Statistics in the Biomedical Sciences for their help with the statistical analysis.

Author contributions

C.S. designed and performed experiments, analyzed and interpreted data, and wrote the manuscript. J.N., F.St. and T.L.B. performed experiments and analyzed data. E.M., C.N., M.B., R.N. and M.R. provided technical support. F.Sa. performed histopathology analysis and edited the manuscript. G.R. supervised research, interpreted data, and edited the manuscript. E.B. supervised research, interpreted data, and wrote the manuscript. A.C. supervised research, interpreted data, wrote the manuscript, and coordinated the study.

Competing interests

A.C. is an inventor on patent applications submitted by Fondazione Telethon or San Raffaele Scientific Institute on LV technology for in vivo use related to the work presented in this manuscript. The remaining authors declare no competing interests.

Additional information

Supplementary information The online version contains supplementary material available at https://doi.org/10.1038/s41467-025-57383-8.

Correspondence and requests for materials should be addressed to Elena Barbon or Alessio Cantore.

Peer review information *Nature Communications* thanks the anonymous reviewers for their contribution to the peer review of this work. A peer review file is available.